Rapid Progression of Ocean Acidification in the California Current System

Nicolas Gruber *et al.*

Science **337**, 220 (2012);
DOI: 10.1126/science.1216773

Science (print ISSN 0036-8075; online ISSN 1095-9203) is published weekly, except the last week in December, by the American Association for the Advancement of Science, 1200 New York Avenue NW, Washington, DC 20005.

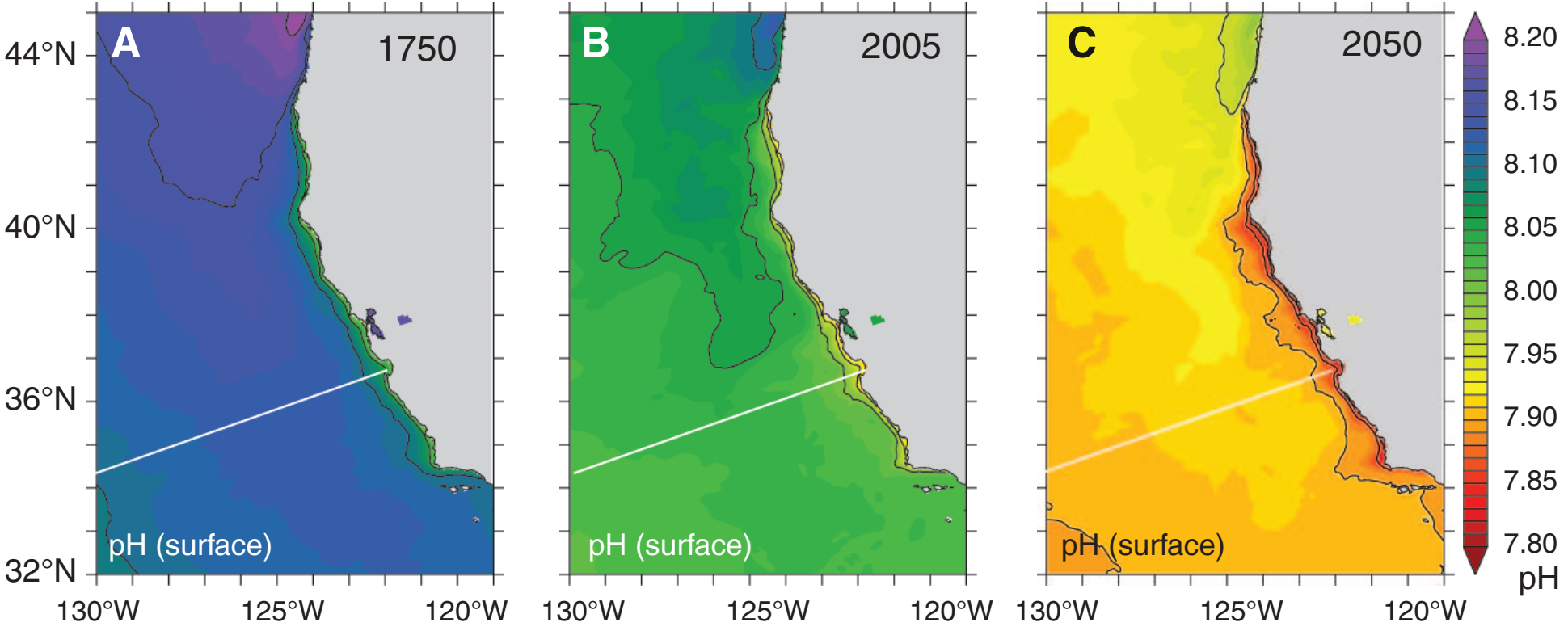
A
1750
pH (surface)
B
2005
pH (surface)
C
2050
pH (surface)
44°N
40°N
36°N
32°N
130°W
125°W
120°W
8.20
8.15
8.10
8.05
8.00
7.95
7.90
7.85
7.80
pH

central California CS [Point Conception (34°35′N) to the California/Oregon border (42°0′N)], where upwelling is strongest.

The model we employ is a California CS set-up of the Regional Oceanic Modeling System (ROMS) (*21*), to which we have coupled a simple nitrogen-based ecosystem model and a full description of the marine inorganic carbon system (see supplementary materials for details and model evaluation) (*22*, *23*). For all simulations, the model is forced with present-day climatological boundary conditions based on observations, except for atmospheric CO_2 and for the lateral boundary conditions of dissolved inorganic carbon. For the preindustrial time-slice simulation, the atmospheric partial pressure of CO_2 (PCO_2) was prescribed at 280 parts per million (ppm), whereas for the transient simulations, atmospheric PCO_2 increased from 364 ppm in 1995 to 492 ppm (B1 scenario) and 541 ppm (A2 scenario), respectively, in 2050. The preindustrial case and the A2 scenario were run with our standard configuration at 5-km horizontal resolution, whereas we employed a coarser-resolution configuration of 15 km to explore the sensitivity of our results to the scenarios.

For the time period between 1750 and 2005, the model simulations suggest that surface-ocean pH decreased from an annual mean of 8.12 ± 0.03 to 8.04 ± 0.03 (1 SD of the spatial mean) for the whole California CS (Fig. 1). Over the same time period, the annual mean surface ocean Ω_{arag} decreased from 2.58 ± 0.19 to 2.27 ± 0.20, reflecting the reduction of the carbonate ion concentration from the titration of the CO_2 that the ocean has taken up from the atmosphere. In the nearshore 10 km of the central California coast, annual mean surface pH and Ω_{arag} in 1750 were already as low as 8.03 ± 0.03, and 1.94 ± 0.14, respectively, reflecting the upwelling of waters with naturally low pH and Ω_{arag} due to the substantial addition of respired CO_2 to these waters. The uptake of anthropogenic CO_2 from the atmosphere until 2005 decreased the surface pH and Ω_{arag} in this region by about the same amount as for the whole domain, yielding annual mean values of 7.95 ± 0.04 and 1.67 ± 0.16, respectively.

For atmospheric PCO_2 following the SRES A2 scenario, our model simulation predicts an even sharper decrease until 2050 to an annual mean surface pH and Ω_{arag} for the whole domain of 7.92 ± 0.03 and 1.77 ± 0.16, respectively, and for the nearshore 10-km environment of the central California CS to 7.82 ± 0.04 and 1.26 ± 0.12, respectively. pH and Ω_{arag} reach even lower values in summer, when upwelling is at its maximum (*13*). In the summer of 2050, for example, our model projects that large stretches of the nearshore 10 km of the central California CS will be undersaturated (see supplementary materials), although the mean Ω_{arag} remains slightly supersaturated (1.05 ± 0.13).

These changes are not confined to the surface ocean, as anthropogenic CO_2 is transported from the surface to depth, causing changes in the carbonate chemistry there as well (Fig. 1, D to F). As a result, the aragonite saturation horizon, which was located at ~350 m in the offshore region and at ~300 m in the nearshore, shoaled generally by ~150 m from 1750 until 2005 and is projected to shoal by another 100 to 150 m between 2005 and 2050. In 2050, the annual mean aragonite saturation horizon is as shallow as 100 m in the offshore region, but shoals to less than 50 m in the nearshore regions in the annual mean. In the summer, the aragonite saturation horizon breaks to the surface in many parts of the central California CS (fig. S4). Thus, ocean acidification will severely reduce the habitat for organisms that are sensitive to the saturation state, particularly for those who cannot tolerate undersaturated conditions for an extended period of time.

The reduction of habitats of organisms sensitive to ocean acidification becomes even more evident when considering the volume of water with a particular range of saturation states within the nearshore 10 km of the central California CS (Fig. 2). In 1750, our model simulates that ~16% of the waters in the euphotic zone (0 to 60 m) in that region had an Ω_{arag} value above 2, with the majority (60%) having an Ω_{arag}

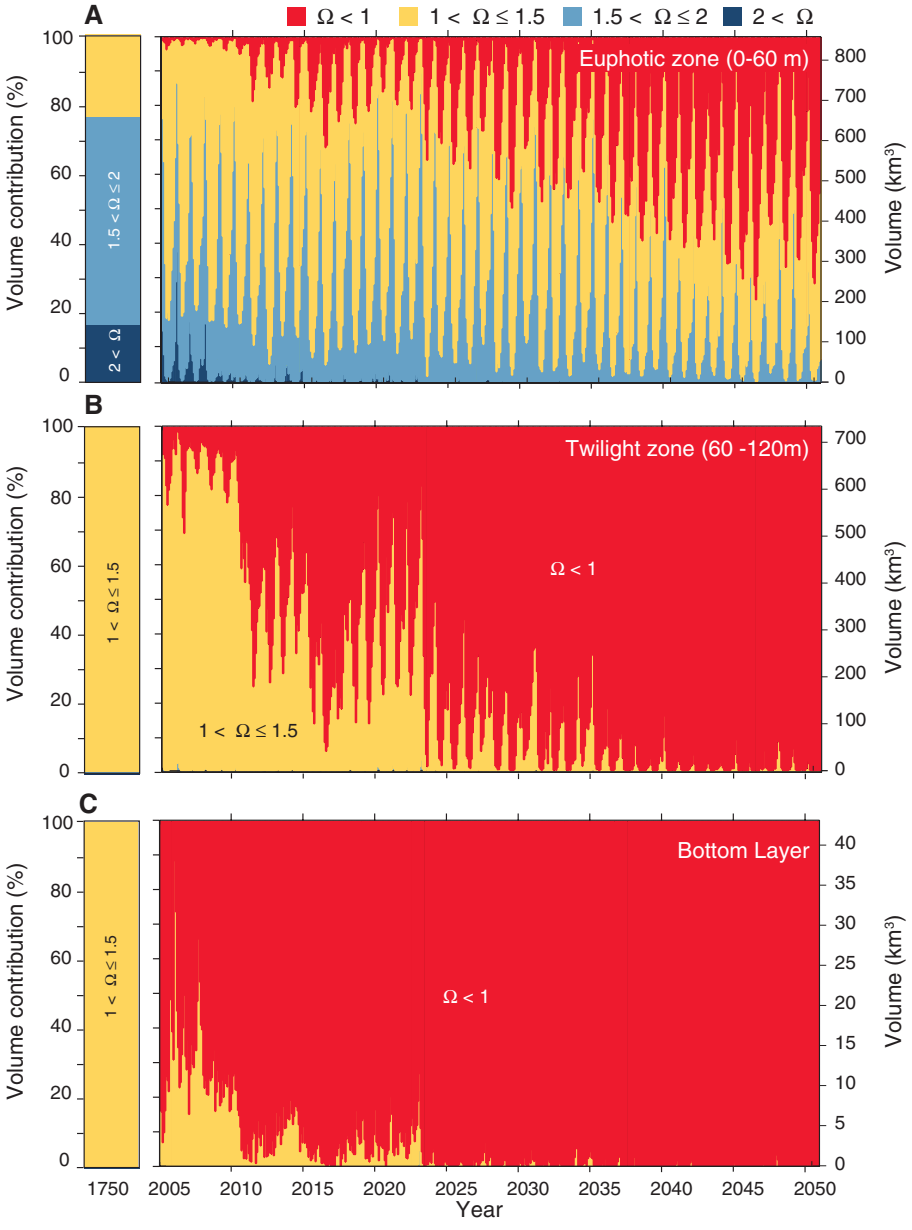

Fig. 2. Temporal evolution of the volume of seawater with a particular Ω_{arag} in the nearshore 10 km of the central California CS for the A2 scenario. The panels depict the evolution (**A**) in the upper 60 m, (**B**) in between 60 and 120 m, and (**C**) in the bottom layer of the model above the shelf sediments (maximum depth: 120 m). Volumes were computed by summing over all regions from Point Conception (34°35′N) to the California/Oregon border (42°0′N).

between 1.5 and 2.0 (Fig. 2A). Only 24% of the waters had an Ω_{arag} between 1.5 and 1.0, and no waters were undersaturated. By 2005, the volume of waters with an Ω_{arag} value greater than 1.5 had dropped to ~20% in the yearly average, with waters with an Ω_{arag} between 1.0 and 1.5 dominating and undersaturated waters appearing seasonally. In the coming decades, waters with $\Omega_{arag} < 1$ are projected to expand substantially in the euphotic zone of the central California CS, occupying more than half of the waters in 2050 in the annual mean. In the summer season, this ratio increases to about 70%, with long stretches of the central coast projected to be undersaturated throughout the euphotic zone (fig. S4). By that time, waters with $\Omega_{arag} > 1.5$ will have largely vanished.

The progression toward widespread and persistent undersaturation in the nearshore 10 km is even more dramatic in the upper twilight zone; that is, in the depth range between 60 and 120 m (Fig. 2B). Though nearly all waters in this depth range were supersaturated with respect to aragonite in preindustrial times, a small but persistent volume of undersaturated waters appears by 2005. Within the next 20 to 30 years, the volume of undersaturated waters quickly expands, and by ~2035 in the SRES A2 scenario, nearly the entire twilight zone of the central California coast will be undersaturated year-round.

Undersaturated conditions became common by 2005 in the bottom layer of the model above the shelf sediments of the central California CS (with water depths ranging between 50 and 120 m) (Fig. 2C). This is a substantial change since preindustrial times, for which the model simulated no undersaturated conditions in this layer. Still, ~30% of this layer remains supersaturated in 2005. Our simulations for the waters above the shelf sediments are consistent with data-based reconstructions for the central Oregon coast (*13*), which also suggest widespread undersaturated conditions for the present but extended periods of supersaturation with regard to aragonite. Such supersaturated conditions are projected to disappear within the next 10 years, so that by the mid-2020s essentially all waters above the shelf sediments will be undersaturated.

Most of these early developments occur regardless of whether atmospheric CO_2 follows the high (A2) or low (B1) CO_2 scenario (see supplementary materials). This lack of sensitivity is due to two factors. First, the two scenarios do not differ substantially in their atmospheric CO_2 levels for the next 20 years; only around 2035 do they begin to deviate more strongly from each other (fig. S5). Second, because surface waters are following the increase in atmospheric CO_2 relatively closely, the primary determinant for the degree of ocean acidification in the upper ocean is the atmospheric CO_2 concentration, not its rate of change. This is well illustrated when the saturation state is plotted as a function of atmospheric P_{CO_2} rather than time (Fig. 3), resulting in nearly identical outcomes for the two scenarios (fig. S7). This means that the timing of when particular chemical thresholds are reached in the upper ocean depends only on when the corresponding atmospheric CO_2 concentration is attained. Our simulation results show that at ~400 ppm, substantial parts of the twilight zone (60 to 120 m) and the habitats along the sea floor on the shelf become undersaturated. Given the present-day atmospheric CO_2 concentration of 390 ppm and the recent rates of increase in atmospheric CO_2 of 1.5 ppm/year or more (*24*), we are virtually certain that a level of 400 ppm will be reached within this decade. When atmospheric CO_2 reaches ~500 ppm, a level that is crossed by ~2040 in the A2 scenario and a little after 2050 in the B1 scenario, the top 60 m in our model begin to experience extended undersaturated conditions. Thus, unless atmospheric CO_2 follows a scenario that is much lower than the low-emission B1 pathway, most of the simulated transitions are bound to happen.

The projected evolution of the upper ocean in the nearshore 10 km of the central California CS toward low Ω_{arag} conditions is similar to that projected for the Southern Ocean and the Arctic Ocean (Fig. 3), which have previously been proposed as the first oceanic regions to become undersaturated (*9*, *18*). The upper twilight zone and the bottom layer of the central California CS become undersaturated even faster than the surface Arctic Ocean, highlighting the imminent nature of reaching this threshold.

The progression of ocean acidification may occur even faster or at lower atmospheric CO_2 concentrations than projected by our model simulations. First, our model tends to overpredict Ω_{arag} in the nearshore regions (see supplementary materials), so that the appearance of certain Ω_{arag} thresholds is probably delayed in the model. A sensitivity test, in which we applied a uniform correction of –0.1 units to Ω_{arag}, revealed that the shifts in the distribution of volumina with a particular saturation state may occur ~10 years earlier than in our standard case (fig. S3). Second, our model is forced with the present-day climatological boundary conditions for all years up to 2050, whereas theoretical considerations (*25*), model simulations (*26*), and historical trends (*27*) suggest that the upwelling favorable winds may increase in the coming decades in response to global warming. This could enhance the upwelling of corrosive water and accelerate the progression toward low Ω_{arag} conditions even further.

Although we are able to project with some confidence the chemical changes associated with the future evolution of ocean acidification in the California CS, the impacts of these chemical changes on organisms, ecosystems, and biogeochemistry remain highly uncertain (*6*, *28*, *29*). The limited evidence available suggests that most aragonite-secreting organisms, such as pteropods or oysters, respond negatively to lowered Ω_{arag} (*30*), with the early-life stages appearing to be particularly sensitive (*31*). We emphasize here the progression toward undersaturated conditions, as this represents a well-established chemical threshold, but

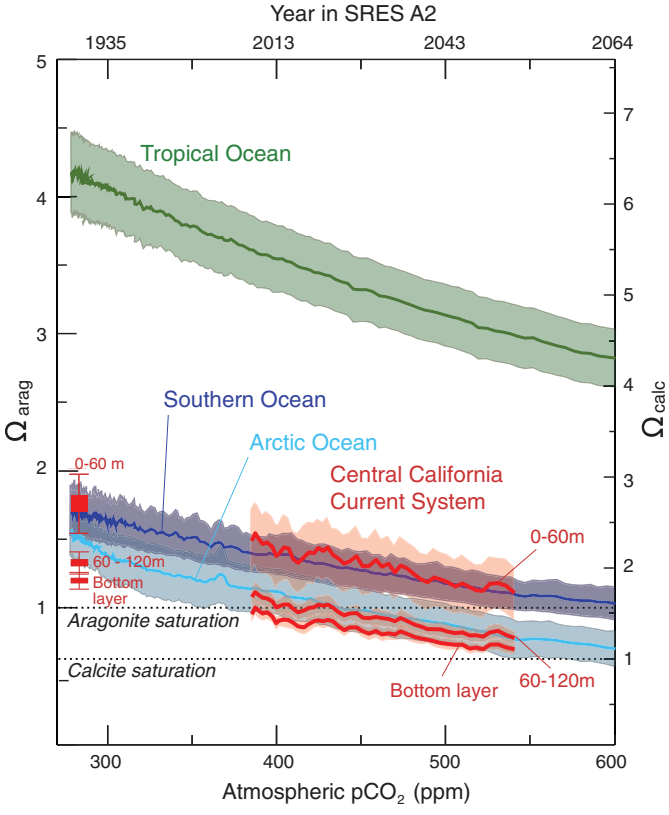

Fig. 3. Temporal evolution of the mean saturation states with regard to aragonite (left *y* axis) and calcite (right *y* axis) in the nearshore 10 km of the central California CS as a function of the atmospheric P_{CO_2} (lower *x* axis) and time (upper *x* axis). The evolutions of three depth layers (0 to 60 m, 60 to 120 m, and the bottom layer of the model above the shelf sediments) are shown. Also shown are the mean evolutions of Ω_{arag} for the tropical ocean, the Southern Ocean, and the Arctic Ocean, as simulated by a global coarse resolution model (*18*). Shaded curves depict the modeled trajectories including ±1 SD of the seasonal variations. All simulations were performed for the A2 scenario.

we must note that none of the organisms studied so far has a simple dose-response curve with a threshold at $\Omega_{arag} = 1$ (*28*). Rather, some organisms or life stages respond negatively at higher Ω_{arag}, whereas others can tolerate undersaturated conditions for some time. In addition, organisms living in the California CS may have had the chance to adapt to the naturally low and variable pH and Ω_{arag} conditions that prevailed before the onset of the industrial revolution, making them potentially less vulnerable to the effects of ocean acidification (*32*). Regardless of these uncertainties associated with the biological response to ocean acidification, our simulation results indicate that the California CS is moving rapidly toward conditions that are well outside the natural range, with frequent or even persistent undersaturation conditions (Fig. 3). Such conditions probably will be challenging to calcifying and other organisms, as well as the fisheries that depend on them (*33*).

Although we focused our study on the changes in Ω_{arag}, ocean acidification alters all aspects of the carbonate chemistry in the ocean, including pH and the concentrations of dissolved CO_2, bicarbonate, and carbonate (*34*), each of which can impact physiological processes and, hence, affect marine organisms and ecosystems (*35*). Yet, the changes in these properties are highly correlated (fig. S7) because they are mechanistically linked through the driver of ocean acidification (i.e., the oceanic uptake of CO_2 from the atmosphere), which increases dissolved CO_2 and bicarbonate but decreases pH, Ω_{arag}, and carbonate with predictable ratios (*34*). Therefore, regardless of whether the parameter affecting a biological process is Ω_{arag} or the dissolved CO_2 concentration, the changes are unprecedented.

In addition, ocean acidification will not be operating in isolation, but its impact could be potentially worsened with synergistic effects of ocean warming and deoxygenation (*35*, *36*), both of which have been noted to occur in the California CS (*37*, *38*) and probably get more severe with time (*39*). Thus, specific attention should be given to the development of ocean acidification in this very rich and productive ecosystem, as well as to some of the other Eastern Boundary Current Systems where similar conditions prevail.

References and Notes

1. W. Stumm, J. J. Morgan, *Aquatic Chemistry: An Introduction Emphasizing Chemical Equilibria in Natural Waters* (Wiley Interscience, New York, ed. 1, 1970).
2. W. S. Broecker, Y.-H. Li, T.-H. Peng, in *Impingement of Man on the Oceans*, D. W. Hood, Ed. (Wiley, New York, 1971), pp. 287–324.
3. J.-P. Gattuso, M. Frankignoulle, I. Bourge, S. Romaine, R. W. Buddemeier, *Global Planet. Change* **18**, 37 (1998).
4. J. A. Kleypas *et al.*, *Science* **284**, 118 (1999).
5. U. Riebesell *et al.*, *Nature* **407**, 364 (2000).
6. S. C. Doney, V. J. Fabry, R. A. Feely, J. A. Kleypas, *Annu. Rev. Mar. Sci.* **1**, 169 (2009).
7. A. Mucci, *Am. J. Sci.* **283**, 780 (1983).
8. R. A. Feely, S. C. Doney, S. C. Cooley, *Oceanography* **22**, 36 (2009).
9. J. C. Orr *et al.*, *Nature* **437**, 681 (2005).
10. B. I. McNeil, R. J. Matear, *Proc. Natl. Acad. Sci. U.S.A.* **105**, 18860 (2008).
11. R. A. Feely, C. L. Sabine, J. M. Hernandez-Ayon, D. Ianson, B. Hales, *Science* **320**, 1490 (2008).
12. C. Hauri *et al.*, *Oceanography* **22**, 60 (2009).
13. L. W. Juranek *et al.*, *Geophys. Res. Lett.* **36**, L24601 (2009).
14. M.-E. Carr, *Deep Sea Res. Part II* **49**, 59 (2002).
15. B. A. Block *et al.*, *Nature* **475**, 86 (2011).
16. R. Costanza *et al.*, *Nature* **387**, 253 (1997).
17. C. Turley *et al.*, *Mar. Pollut. Bull.* **60**, 787 (2010).
18. M. Steinacher, F. Joos, T. L. Frölicher, G.-K. Plattner, S. C. Doney, *Biogeosciences* **6**, 515 (2009).
19. F. Joos, T. L. Frölicher, M. Steinacher, G.-K. Plattner, in *Ocean Acidification*, J.-P. Gattuso, L. Hansson, Eds. (Oxford Univ. Press, Oxford, 2011), chap. 14, pp. 272–290.
20. N. Nakicenovic *et al.*, *Special Report on Emissions Scenarios: A Special Report of Working Group III of the Intergovernmental Panel on Climate Change* (Cambridge Univ. Press, New York, 2000).
21. A. F. Shchepetkin, J. C. McWilliams, *Ocean Model.* **9**, 347 (2005).
22. N. Gruber *et al.*, *Nat. Geosci.* **4**, 787 (2011).
23. Z. Lachkar, N. Gruber, *Biogeosciences* **8**, 2961 (2011).
24. P. Tans, R. F. Keeling, Recent Mauna Loa Data, Electronic Data (National Oceanic and Atmospheric Administration Earth System Research Laboratory, Scripps Institution of Oceanography, Boulder, CO, 2012); www.esrl.noaa.gov/gmd/ccgg/trends/.
25. A. Bakun, *Science* **247**, 198 (1990).
26. N. S. Diffenbaugh, M. A. Snyder, L. C. Sloan, *Proc. Natl. Acad. Sci. U.S.A.* **101**, 27 (2004).
27. D. Gutiérrez *et al.*, *Geophys. Res. Lett.* **38**, L07603 (2011).
28. K. J. Kroeker, R. L. Kordas, R. N. Crim, G. G. Singh, *Ecol. Lett.* **13**, 1419 (2010).
29. J. P. Barry, S. Widdicombe, J. M. Hall-Spencer, in *Ocean Acidification*, J.-P. Gattuso, L. Hansson, Eds. (Oxford Univ. Press, Oxford, 2011), chap. 10, pp. 192–209.
30. V. J. Fabry, B. A. Seibel, R. A. Feely, J. C. Orr, *ICES J. Mar. Sci.* **65**, 414 (2008).
31. A. Barton, B. Hales, G. G. Waldbusser, C. Langdon, R. Feely, *Limnol. Oceanogr.* **57**, 698 (2012).
32. M. D. Ohman, B. E. Lavaniegos, A. W. Townsend, *Geophys. Res. Lett.* **36**, L18608 (2009).
33. S. R. Cooley, S. C. Doney, *Environ. Res. Lett.* **4**, 024007 (2009).
34. J. C. Orr, in *Ocean Acidification*, J. P. Gattuso, L. Hansson, Eds. (Oxford Univ. Press, Oxford, 2011), chap. 3, pp. 41–66.
35. H. O. Pörtner, *Mar. Ecol. Prog. Ser.* **373**, 203 (2008).
36. N. Gruber, *Philos. Trans. R. Soc. London Ser. A* **369**, 1980 (2011).
37. S. J. Bograd *et al.*, *Geophys. Res. Lett.* **35**, L12607 (2008).
38. F. Chan *et al.*, *Science* **319**, 920 (2008).
39. R. F. Keeling, A. Kortzinger, N. Gruber, *Annu. Rev. Mar. Sci.* **2**, 199 (2010).

Acknowledgments: This work was supported by ETH Zürich and the European Project on Ocean Acidification, which received funding from the European Community's Seventh Framework Programme (FP7/2007-2013) under grant agreement no. 211384. T.L.F. was supported by the Carbon Mitigation Initiative project at Princeton Univ., sponsored by BP and Ford Motor Company. We thank J. C. McWilliams and his group at the Univ. of California Los Angeles for the long-term collaboration on the development of ROMS.

Supplementary Materials

www.sciencemag.org/cgi/content/full/science.1216773/DC1
Supplementary Text
Figs. S1 to S8
References

17 November 2011; accepted 30 May 2012
Published online 14 June 2012;
10.1126/science.1216773

Clovis Age Western Stemmed Projectile Points and Human Coprolites at the Paisley Caves

Dennis L. Jenkins,[1]*† Loren G. Davis,[2]* Thomas W. Stafford Jr.,[3,4]* Paula F. Campos,[3,5]* Bryan Hockett,[6] George T. Jones,[7] Linda Scott Cummings,[8] Chad Yost,[8] Thomas J. Connolly,[1] Robert M. Yohe II,[9] Summer C. Gibbons,[9] Maanasa Raghavan,[3] Morten Rasmussen,[3] Johanna L. A. Paijmans,[10] Michael Hofreiter,[10] Brian M. Kemp,[11] Jodi Lynn Barta,[11,12] Cara Monroe,[11,13] M. Thomas P. Gilbert,[3] Eske Willerslev[3]*†

The Paisley Caves in Oregon record the oldest directly dated human remains (DNA) in the Western Hemisphere. More than 100 high-precision radiocarbon dates show that deposits containing artifacts and coprolites ranging in age from 12,450 to 2295 ^{14}C years ago are well stratified. Western Stemmed projectile points were recovered in deposits dated to 11,070 to 11,340 ^{14}C years ago, a time contemporaneous with or preceding the Clovis technology. There is no evidence of diagnostic Clovis technology at the site. These two distinct technologies were parallel developments, not the product of a unilinear technological evolution. "Blind testing" analysis of coprolites by an independent laboratory confirms the presence of human DNA in specimens of pre-Clovis age. The colonization of the Americas involved multiple technologically divergent, and possibly genetically divergent, founding groups.

Despite increasing evidence for pre-Clovis sites in North and South America (*1*–*6*), debate continues as to whether the technological tradition that led to Clovis was the first to arrive in the Americas. Was Clovis the first in a long, unilinear technological evolution spreading throughout the Americas? Or were other Pleistocene technological complexes involved (*6*–*10*)? In the American Far West, the Western Stemmed Tradition (WST) is recognized as the oldest nonfluted lithic technology. Stemmed points were present earlier in East